

Optimization of Landing Gear Fairings

Final Report

Group7

Daniel Ablog, Michael Fuget, Seunghyun Ko, and Keisuke Tsujita

AA 322 Aerospace Laboratory II

WILLIAM E. BOEING DEPARTMENT OF AERONAUTICS & ASTRONAUTICS

University of Washington

Seattle, Washington, 98195-2400

2014-05-05

Wind tunnel and flow visualization experiments were conducted to determine the aerodynamic effects of landing gear fairings of varied length at different angles of attack in both the University of Washington 3x3 Wind Tunnel and water tunnel. This experiment utilized a 1:3 scale model of the actual fairing and ratios of length 0.7d, 1.0d, 1.14d, 1.5d, and 2d. Water tunnel testing of the fairings provided a means to flow visualization around each model. Dye was injected in front of the models to see the flow around the fairings. For most models, the flow separated before reaching the fairing and therefore, the fairing had no aerodynamic effect. However, for the longer fairings, flow remained attached to the fairings for a longer period of time before separating. In concordance, wind tunnel tests showed that longer fairings generally had less drag than those of the covered fairing and individual wheel. These results indicate that attaching longer fairings to the wheel of a landing gear substantially reduces drag in comparison to that of shorter fairings.

Nomenclature

A	Axial Force (lb)
c	Chord length (in)
C	Coefficients
d	Diameter of wheel (in)
D	Drag(lb)
l	Length of the fairings (in)
L	Lift(lb)
M	Moment(in-lb)
N	Normal Force(lb)
q	Dynamic Pressure(lb/ft ²)

Re	Reynolds Number
S	Surface area of test samples (in^2)
t	Thickness (in)
α	Angle of attack ($^\circ$)
ρ	Density of air (slug/ft^2)
μ	absolute viscosity coefficient ($\text{slug}/(\text{ft}^*\text{s})$)

Subscript

A	Axial
D	Drag
L	Lift
M	Moment
N	Normal

I. Introduction

Small airplanes, such as Cessna 150, cover their non-retractable landing gear wheels with the streamlined fairings which is also known as wheel pants while large airplanes have a retractable landing gear to decrease the drag associated with the landing gear during their flight.



Fig. 1: Landing gear fairing of Cessna 150

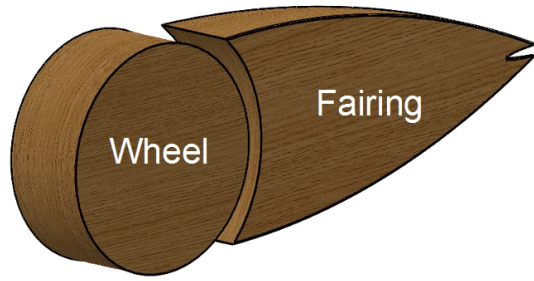


Fig. 2: Fairing design that does not cover the wheel

Currently, the fairings of non-retractable landing gear cover the top half of the wheel as shown in Fig. 1.¹ Previously, the drag of several types of existing fairings were measured by Herrnstein and Biermann.²

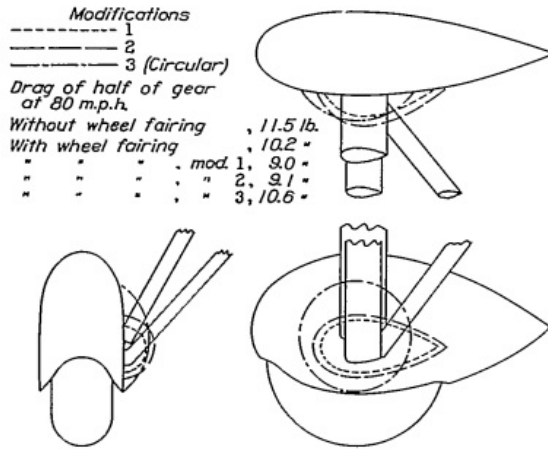


Fig. 3: The Smallest Drag Fairing Configuration

Should I have this part here or in the theory? From the experiment, the fairing shown in Fig. 3 with modification 2 had the smallest drag among the six types of fairings tested. The other configurations of fairing tested are shown in Appendix A. Herrnstein and Biermann² concludes that the fairing which covered both sides of the wheel and had minimal frontal area was most effective in reducing drag. Although the fairings reduce the drag, they are the extra weight added to the airplane, which should be minimized. One way to reduce the weight of a landing gear fairing is to utilize the new design of the fairing which does not

cover the wheel as shown in Fig. 2. The new design of the fairing does not increase the frontal area and may reduce the weight while keeping the drag performance similar to that of the existing fairing. The purpose of this project is to measure the aerodynamic forces and visualize the flows around the fairings with five different lengths using the configuration shown in Fig. 2, a fairing with the existing configuration of fairings as shown in Fig. 1, and a wheel without a fairing. The results are compared to determine the differences in drag and volume.

II. Theory

A. Assumptions and Simplifications

Several assumptions and simplifications were made for the test samples. First, the test model can consist of only a wheel and fairing behind the wheel. Also, although a real wheel is made of several parts and different materials, a circular cylinder, whose ratio of thickness and diameter is the same as that of a real wheel, can model the wheel. Also, the test models can be modeled by any materials as long as they are consistent for all models. These simplifications are valid because the purpose of the project is only to investigate the effect of the variation of length of the fairings. In addition, the assumption that the wheel modeled by a cylinder does not rotate was made because wheels on a Cessna 150 do not rotate during cruising conditions.

B. Physics

Title of the subsection must be changed Aerodynamic forces exerted by the flow of air are due to the pressure distribution of the surface and shear stress on the surface.³

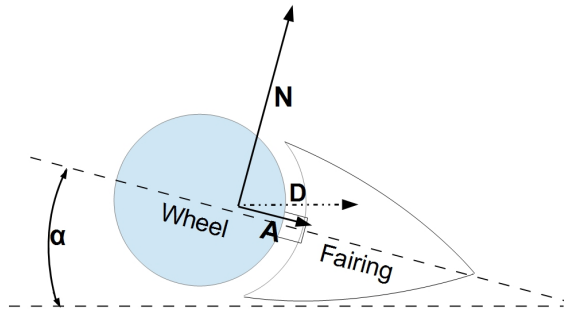


Fig. 4: Aerodynamic forces on the test sample

The sting mount in the 3x3 wind tunnel measures the normal and axial force shown in Fig. 4. Drag at a certain angle of attack can be calculated from normal and axial forces as follows.

$$D = N \sin \alpha + A \cos \alpha \quad (1)$$

The Reynolds number, which is strongly associated with drag, can be found by.³

$$Re = \frac{\rho V_\infty c}{\mu} = \frac{\rho V_\infty (d + l)}{\mu} \quad (2)$$

Since drag depends on the dynamic pressure and projected area, drag coefficient coefficient are defined as

$$C_D = \frac{D}{q_\infty S} = \frac{D}{q_\infty td} \quad (3)$$

As explained in Section II-A, the test sample models the wheel by a circular cylinder, whose pressure drag is higher than the friction drag.⁴ The pressure drag is produced by the pressure difference between the front and back side of the cylinder. This difference is caused by the wake formed behind the cylinder.⁵

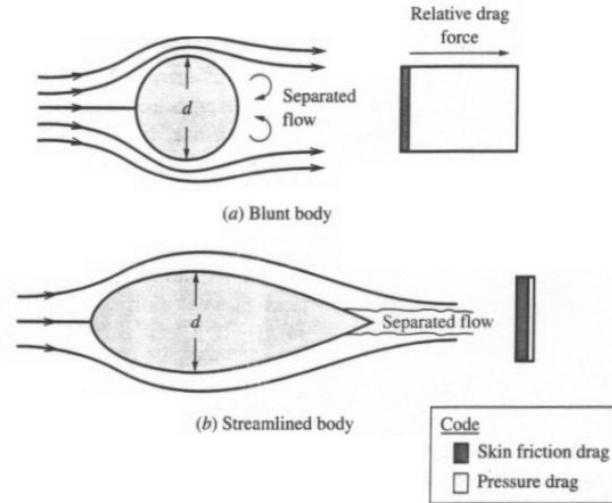


Fig. 5: Flow over a blunt body and streamlined body

The drag characteristic of the blunt body, such as a circular cylinder, and the streamlined body are shown in Fig. 5. The blunt body has large pressure drag caused by the wake formed behind the body due to the flow separation. The new model shown in Fig. 2 uses the wheel as the front portion and itself as the back portion of the streamlined body. This may lead to less pressure drag compared to the case in which only the wheel is employed.

C. Previous work related to the design and dimensions of the fairings

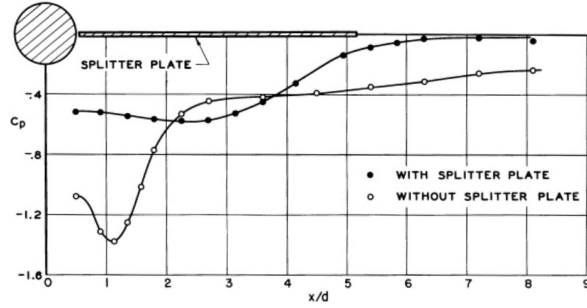


Fig. 6: Pressure distribution over the cylinder with splitter plate behind

Roshko⁶ states that when a cylinder is placed in front of a flat splitter plate which has a length of 5 times the diameter of the cylinder, as shown in Fig. 6, the drag coefficient of the cylinder is reduced from 1.1 to 0.7. Fig. 6 shows the pressure distribution behind the circular cylinder with splitter plate and that without splitter plate. The splitter plate is effective in reducing the pressure drop behind the circular cylinder. Also, Roshko states that by using a splitter plate with a length of 1.14 times the diameter, the vortex shedding frequency varies depending on the location of the plate whereas the drag did not decrease.⁶ These previous work indicate that the length of the splitter plate is what affects the reduction in drag. The length of the splitter plate was used as the reference length in the project as explained in the Section III-A.

III. Designing and Fabrication of the Models

A. Designing of the test models and Determining the test conditions

The dimensions of the wheel were determined based on the actual wheel used. The Cessna 150 employs a wheel whose diameter is 15 in and thickness is 6 in.⁷ Due to the size of the wind tunnel, the wheel's diameter was scaled down to be 5 in, and the thickness was decided to be 2 in in order to match the ratio of diameter and thickness of the actual wheel.

The lengths of the fairings to be tested were chosen as $0.7d$, $1.0d$, $1.14d$, $1.5d$, and $2.0d$. Even though the previous work described in Section III shows that the splitter plate, whose length is $5d$, placed behind the circular cylinder is effective in reducing the drag,⁶ the largest length was decided to be $2d$. This decision was made because the fairing may touch the ground during the takeoff or landing if the length is too long. Other dimensions, which are kept constant among the model fairings, were also decided. The width of the fairing was decided to be the same as the thickness of the wheel because the previous experiment by Herrnstein and Biermann² described in Section II shows that fairing with the smallest frontal area had the lowest drag. The spacing between the fairing and the wheel was chosen to be 0.5 in, which corresponds to 1.5 in in the real scale. This spacing was chosen because certain clearance between the fairing and the wheel is required in case of landing on muddy ground. The height of the fairing was decided to be 80% of the diameter of the wheel to allow the smooth transition of the flow from the wheel to the fairing.

It is ideal to execute the experiments under the dynamically similar condition, represented by the Reynolds number. First, the Reynolds number of the flow which the actual landing gear experiences was calculated. The cruising speed of the Cessna 150 at altitude of 7000 ft is 117 mph.⁸ The Reynolds number for its wheel at that speed and altitude was calculated with Eq. 2 with the cruising speed and properties of air at 7000 ft listed in Table. 1. The

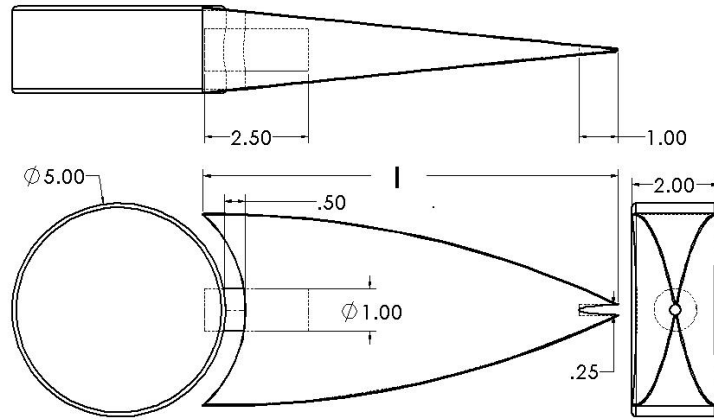
Table 1: Properties of Air at 7000 ft

Properties	Values
Temperature(R°)	493.73
Pressure(lb/ft^2)	1.6331×10^3
Density($slug/ft^3$)	1.9270×10^3

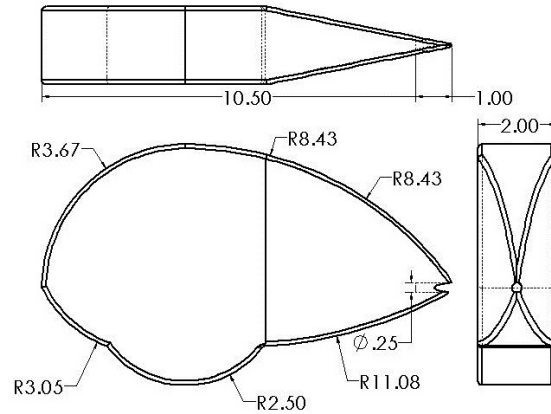
viscosity of air was found by interpolating the data in Table. 6 in Appendix B. The Reynolds number was calculated to be 1.13×10^6 with Eq. 2.

However, due to the limitation of the testing facilities, it was not possible to conduct the experiment with the same Reynolds number. The air speed and water speed of the testing facilities were limited as well as the maximum size of the models which can be used. The 3x3 wind tunnel can not be operated above 45 psf of dynamic pressure. Under the standard atmosphere at sea level, the Reynolds number was calculated to be only 5.0×10^5 with Eq. 2. The Reynolds number in water tunnel was also calculated to be 6.5×10^4 .

The dimensions of the test samples are shown in Fig. 7



(a) Wheel with new model of fairing. $l = 0.7d, 1.0d, 1.14d, 1.5d$ or $2.0d$. Unit is inch



(b) Current design of the fairing. For simplicity, the fairing and the wheel was designed as one body. Unit is inch

Fig. 7: The design of the new and current fairing test samples

Because the experiments are planned to be executed in the 3x3 wind tunnel and in the water tunnel, a mount must be created for each tunnel. The CAD drawing for the sting mount, which measures the aerodynamic forces and moments, was obtained to design the extension mount for the wind tunnel. A CAD model of the extension mount for the sting mount in the 3 x 3 wind tunnel was created as shown in Fig. 8.

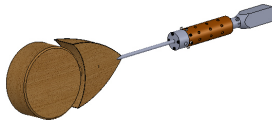


Fig. 8: Extension mount design for wind tunnel testing

In addition, the mount for the experiments in the water tunnel was designed as shown in Fig. 9. These configurations were chosen to minimize the effect of the mount on the experiments.

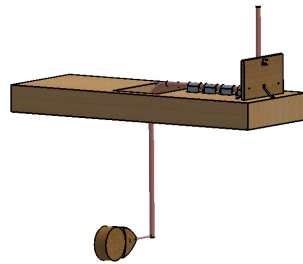


Fig. 9: Mount design for water tunnel testing

B. Fabrication of test samples

The materials purchased for fabrication are listed in Appendix B. A model wheel and five fairings with different lengths were fabricated from wood. The test samples were cut with the band saw in the machine shop in the Mechanical Engineering Department. The fabricated test samples are shown in Fig. ???. Making a perfectly symmetrical test samples was extremely difficult, and the thickness of the fairings became slightly smaller than what was originally designed as they were sanded to be tapered. After sanding sealer was applied, the models were waterproofed for the experiment in the water tunnel. The machine shop in the Mechanical Engineering Department and Aeronautics and Astronautics Department were used to fabricate the test samples. The 3×3 Wind Tunnel and Water Tunnel were used to conduct the experiments.

The test samples used in the water tunnel and the wind tunnel are shown in Fig. ??.

IV. Experimental Apparatus

The setup of the experiment in the water tunnel and in the wind tunnel are included in Fig. 11a and Fig. 11c, respectively. The mount shown in Fig. 9 was used to hold the test samples and change angles of attack in the water tunnel.

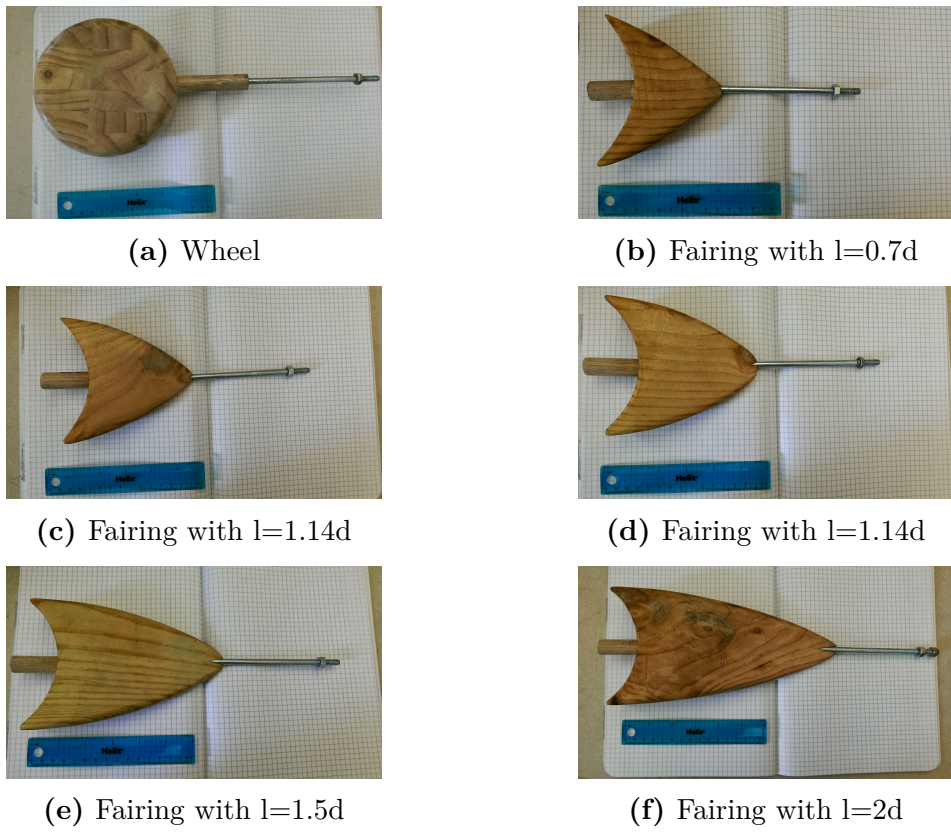
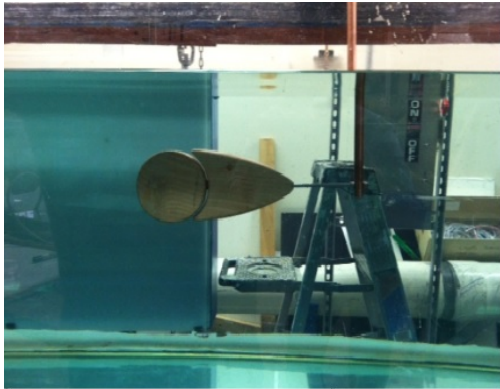


Fig. 10: Fabricated Test Samples

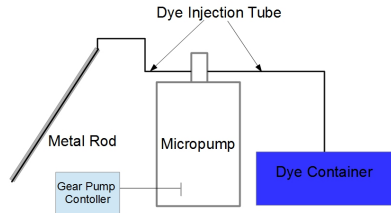
Table 2: Apparatus used in the water tunnel

Equipment
Water Tunnel
Dye Injection Tube
Lucks Color Blue
Lucks Color Green
Micropump
Gear Pump Controller
Water Tunnel Mount

Table 2 includes the apparatus used for the flow visualization in the water tunnel experiment.



(a) Experimental Setup for the Water Tunnel



(b) Dye Injection System for the Water Tunnel Experiment



(c) Experimental Setup for the Wind Tunnel

Fig. 11: Experiment Setups

Table 3: Apparatus used in the 3×3 wind tunnel

Equipment	Model
3x3 Wind Tunnel Attachment Mount	

Table 3 includes the apparatus used for the drag measurements in the 3×3 wind tunnel.

V. Procedure

A. Water Tunnel Test

The bare wheel and the fairings attached to the wheel were tested in the water tunnel to visualize the flows around the samples. One of the injection port of the Micropump was connected to the dye container with a dye injection tube. The other injection port was connected with the dye injection tube, which was attached to the metal rod for the dye injection in the water tunnel. The gear pump controller was connected to the Micropump to

control the amount of dye to be injected. Schematic of the dye injection system is shown in Fig. 11b. The test samples were attached to the water tunnel mount. The following angles of attack were tested: -10° , -7° , -2° , 0° , 10° , 15° , 20° , and 20° . While the experiment, the dye injecting tube attached to the metal rod was moved by hand to see the flow over and under the test samples. In order to analyze the flows over and under the test samples, green dye and blue dye were injected from the top surface and bottom surface of the test samples, respectively. However, there was not enough green dye for all runs thus blue dye was injected from both top and bottom of the flows. The frequency of the water tunnel was set to 50 Hz, which corresponds to the 50cm/sec. The conversion chart between the frequency and the water speed is in Appendix.... Movies were taken to analyze the flows.

B. Wind Tunnel Test

The atmospheric pressure was recorded. The test samples were attached to sting mount by the attachment mount as shown in Fig. 11c with aluminum tape to reinforce the attachment. Angles of attack was changed from 0° to 20° with increment of 2° . For each run, the dynamic pressure was gradually increased from zero to near 45 psf. LabView was used to record dynamic pressure, temperature, axial forces, and normal forces.

VI. Discussion of Results

A. Measurement of drag

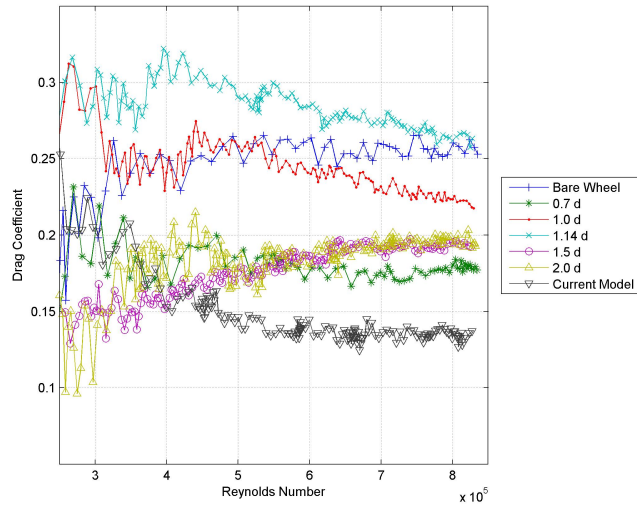


Fig. 12: Drag Coefficient measured at $\alpha = 0$ for each test sample with various Reynolds number

Fig. 12 is the plot of the drag coefficient measured at $\alpha = 0$ with Reynolds number from $Re = 3.5 \times 10^5$ to 7.0×10^5 . Except in the lower Reynolds number range, all of the samples with fairing had the lower coefficient of drag than that with the bare wheel. The current model of the fairing and the test sample with $l = 0.7\text{ }d$, $l = 1.0\text{ }d$, and $l = 1.14\text{ }d$ of fairing,

showed slight decrease as the Reynolds number increased. On the other hand, the sample with $l = 1.5 d$, $l = 2.0 d$ of fairing showed slight increase in drag coefficient. At zero angle of attack, which is typical in cruise, the current model of fairing showed the best aerodynamic performance over the range of Reynolds number tested.

Table 4: The Coefficient of drag and percent decrease compared to the bare wheel model for low and high Re with weight ratio of the models at zero angle of attack

	Low Re		High Re		Weight Ratio(%)
	C_d	% Decrease	C_d	% Decrease	
Bare Wheel	0.245	-	0.256	-	0
0.7 d	0.186	24.2	0.177	30.9	23.1
1.0 d	0.255	-3.83	0.226	12.0	35.8
1.14 d	0.308	-25.6	0.269	-4.76	42.4
1.5 d	0.165	32.9	0.193	24.9	56.7
2.0 d	0.194	21.0	0.196	23.6	73.4
Current Model	0.157	36.0	0.135	47.4	1

Table 4 includes the C_d and the percent decrease compared to the bare wheel for each low and high Reynolds number with the weight ratio of the fairing compared to the current model at zero angle of attack.

Among the new design of the fairings, at lower Reynolds number, the fairing with the length of $1.50 d$ had the best aerodynamic performance as shown in Fig. ???. On the other hand, the at higher Reynolds number, the fairing with the length of $0.7 d$ was the lowest coefficient of drag. Overall, length The all the models with new fairing design had better performance except the sample with $l = 1.14 d$ of fairing in the high Reynolds number range. For most of the

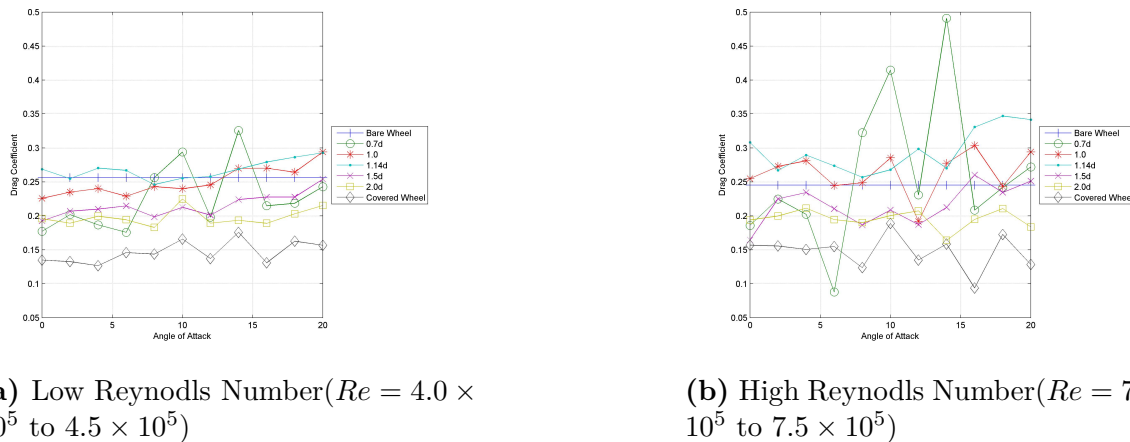


Fig. 13: Avarage drag Coefficient measured at lower and higher Reynolds number for each test sample with various angles of attack

The drag coefficients for each fairing were plotted against varying angle of attack. Low

Reynold's number testing data is shown in Fig. 13a and High Reynold's number data in Fig. 13b. The general trend shown in the plot is the increase in the coefficient of drag of all models except the bare wheel with increasing angle of attack. In addition from these plots, it can be seen that among the new design of the fairings, the 2d length fairing generally had the lowest drag coefficient compared to those of the individual wheel alone over the range of the angle of attack. However, the covered fairing still had the best aerodynamic performance with the lowest drag coefficients. This was expected as the covered fairing has no separation between the wheel and after body, allowing for less chance of flow separation. Regardless of this fact, it is still good to note that the weight difference between these fairings and the covered fairing is substantial despite having a slight difference in drag performance.

I am not sure about this. Also evident in Fig. 13 is the decrease in drag coefficient, going from the low Reynold's number data to the high Reynold's number data. A comparison between these two plots shows that, in general, the drag coefficient reduces as the Reynold's number is increased. This is due to turbulent flow which occurs in higher Reynold's number flight. Turbulent flows remain attached to the fairing surface longer than flow during low Reynold's number. This increases pressure acting on the rear of the model and therefore, reduces the drag component of the landing gear.

This may not be correct. The outlier in the wind tunnel experiment was the 1.14d fairing. Drag coefficient for this fairing came out to be much higher than the 1d fairing. Some data points even exceeded those of the individual wheel. This may be attributed to manufacturing error such as having substantial roughness or improper shaping of the model.

B. Flow Visualization

Flow over the test samples for each run is shown in Fig.XX. The flow over the bare wheel is shown in Fig.XX.

As indicated by Fig.XX, when the test sample has a positive angle of attack, the flow bottom of the wheel goes in the gap between the wheel and fairing, moving up to the top side of the test model. When the flow from the bottom side mixes with the flow on top of the sample, the separation occurs. When the test sample has a negative angle of attack, the flow on top side of the sample moves in the gap and causes the flow to separate on the bottom side of the model.

In the case of model having zero and small angles of attack, the flow stays attached on the wheel and fairing as shown in Fig.XX.

When the wheel has large angles of attack, the pressure difference between the top and bottom sides of the models is large, causing the flow suction into the gap.

VII. Conclusion

As of May 5th, the design of test samples and mounts is completed. Also, fabrication of the test models has begun. However, experiments have not been executed, and therefore, data cannot be presented.

References

- ¹Federal Aviation Administration, "Aircraft Landing Gear Systems", *Aviation Maintenance Technician Handbook-Airframe*, Vol. 2, 2012, Chapter 13.
- ²Herrnstein, H., and Biermann, D., "The drag of airplane wheels, wheel fairings, and landing gears - I" NACA Report-485., 1935.
- ³Anderson, J. D., "Basic Aerodynamics", *Introduction to Flight*, 7th ed, McGraw-Hill, New York, NW. 2012, pp 134-288.
- ⁴Anderson, J. D., "Introduction to the Fundamental Principles and Equations of Viscous Flow", *Fundamentals of Aerodynamic*, 3rd ed, McGraw-Hill, New York, NW. 2001, pp 713-745.
- ⁵Anderson, J. D., "Fundamentals of Inviscid, Incompressible Flow", *Fundamentals of Aerodynamic*, 3rd ed, McGraw-Hill, New York, NW. 2001, pp 177-275.
- ⁶Roshko, A., "On the Wake and Drag of Bluff Bodies", *AIAA Journal*, Vol. 22, No. 2 (1955), pp. 124-132.
- ⁷The Goodyear Tire & Rubber Company, "Flight Special II" *GOODYEAR Aviation Tires* ,Ohio, 2013 [<http://www.goodyearaviation.com/cfmx/web/aviattiresel/details.cfm?sortorder=35#FB> ACCESSED 4/28/2014]
- ⁸Cessna Sales and Service, "Description and Operating Details", *Model 150 Owner's Manual*, Wichita, Kansas, 1968.
- ⁹Anderson, J. D., "Standard Atmosphere, English Engineering Units", *Introduction to Flight*, 7th ed, McGraw-Hill, New York, NW, 2010, pp 770-773.
- ¹⁰Cengel, Y. A., "Conversion Factors", *Thermodynamics: Engineering Approach*, 7th ed, McGraw-Hill, New York, NW, 2012, pp 655-687.
- ¹¹The Engineering ToolBox, "Absolute and kinematic viscosity of air at temperatures ranging -40 - 1000 °C (-40 - 1500 °F) at standard atmospheric pressure - Imperial and SI Units" [http://www.engineeringtoolbox.com/air-absolute-kinematic-viscosity-d_601.html ACCESSED 5/2/2014]

Appendix

A. Fairings tested by Herrnstein and Biermann

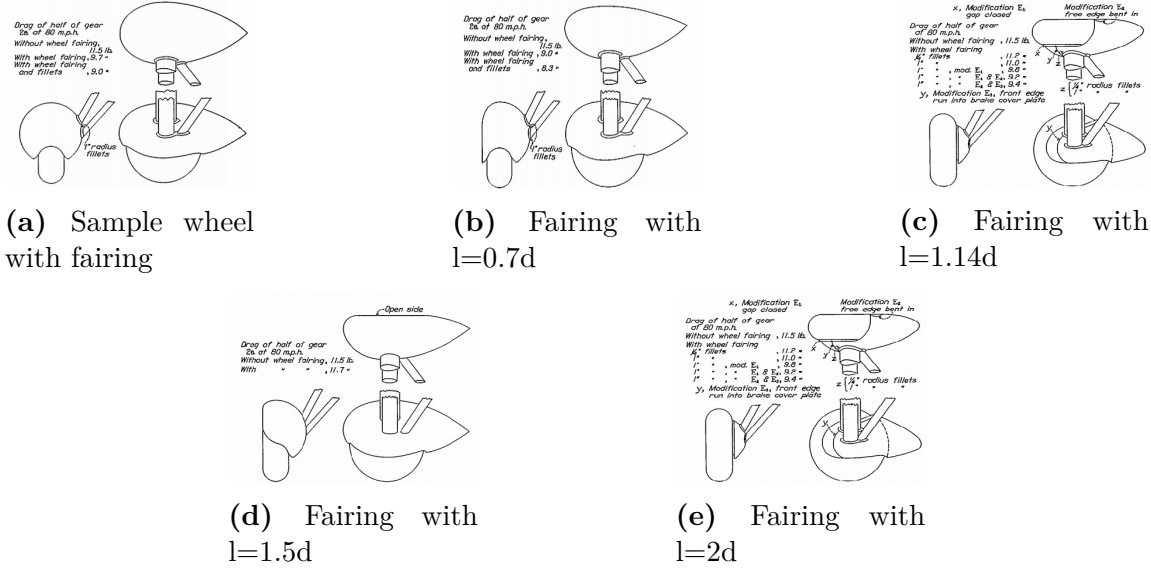


Fig. 14: Other types of fairings tested by Herrnstein and Biermann²

B. Item Purchased

Table 5: Items Purchased

4-4x6 12 feet wooden beams
Sanding Sealer
1-1/4 in metal rod
1-3/8 in metal rod
1-1/2 in metal rod
2-3/4 in brass pipes 5 feet long
3-3/4 in brass elbows
1/2 in dowel
5/8 in dowel
3/4 in dowel
epoxy
screws
